Analysis of scanning tunneling microscopy images of the charge-density-wave phase in quasi-one-dimensional $Rb_{0.3}MoO_3$

E. Machado-Charry, P. Ordejón, and E. Canadell*
Institut de Ciència de Materials de Barcelona (ICMAB-CSIC), Campus de la UAB, 08193 Bellaterra, Spain

C. Brun and Z. Z. Wang
Laboratoire de Photonique et de Nanostructures, CNRS, route de Nozay, 91460 Marcoussis, France
(Received 9 March 2006; revised manuscript received 11 August 2006; published 25 October 2006)

The experimental scanning tunneling microscopy (STM) images for the charge-density-wave (CDW) phase of the blue bronze $Rb_{0.3}MoO_3$ have been successfully explained on the basis of first-principles density functional theory calculations. Although the density of states near the Fermi level strongly concentrates in two of the three types of Mo atoms (Mo_{II} and Mo_{III}), the STM measurement mostly probes the contribution of the uppermost O atoms of the surface, associated with the Mo_IO_6 octahedra. In addition, it is found that the surface concentration of Rb atoms plays a key role in determining the surface nesting vector and hence, the periodicity of the CDW modulation. Significant experimental inhomogeneities of the $\boldsymbol{b}^*$ surface component of the wave vector of the modulation probed by STM are reported. The calculated changes in the surface nesting vector are consistent with the observed experimental inhomogeneities.

DOI: 10.1103/PhysRevB.74.155123 PACS number(s): 71.45.Lr, 68.37.Ef, 71.20.−b, 73.20.−r

I. INTRODUCTION

Low-dimensional molybdenum and tungsten oxides and bronzes have been the focus of much attention because of the charge-density wave (CDW) and associated phenomena they exhibit.[1] The blue bronzes, $A_{0.3}MoO_3$ (A=K,Rb,Tl), are quasi-one-dimensional metals exhibiting a metal-to-insulator transition and are among the most intensely studied of these materials. Their crystal structure is built from MoO_3 layers in between which the cations reside (Fig. 1).[2] Despite many attempts, observation of the CDW in these materials by scanning tunneling microscopy (STM) has been elusive. Only very recently, high resolution STM images of an *in situ* cleaved $(\bar{2}01)$ surface of the rubidium blue bronze, $Rb_{0.3}MoO_3$, have been obtained at low temperature and in ultra-high vacuum (UHV).[3] Both the molecular lattice and the CDW superlattice were observed simultaneously at temperatures well below the CDW transition temperature.

Comparison of these images with previous first-principles density functional theory (DFT) calculations for the bulk,[4] as well as with experimental information of the bulk structure of the modulated phase,[5] is quite puzzling. For instance, some of the most intense features of the STM images are associated with the Mo_IO_6 octahedra (Fig. 1), which are only weakly involved in the CDW transition according to the superlattice structural study.[5] Parenthetically, the Mo_I orbitals have a minor contribution to the states near the Fermi level according to the first-principles calculations.[4] These and related observations prompted the present work. Here we report a first-principles study of the STM images of modulated and nonmodulated $Rb_{0.3}MoO_3$ with special emphasis on the influence of the alkali atoms at the surface. This is a key issue when trying to directly observe the CDW modulations in materials such as low-dimensional bronzes, because it may affect the surface nesting vector and hence, the nature of the modulation observed. We also report new experimental results concerning inhomogeneities in the surface modulation wave vector providing support for the analysis. Finally, a clearcut understanding of the STM images for the blue bronze emerges from this work.

II. CALCULATION METHOD AND BAND STRUCTURE

The present calculations were carried out using a numerical atomic orbitals DFT[6,7] approach, which has been developed and designed for efficient calculations in large systems and implemented in the SIESTA code.[8] We have used the generalized gradient approximation to DFT and, in particular, the functional of Perdew, Burke, and Ernzerhof.[9] Only the valence electrons are considered in the calculation, with the core being replaced by nonlocal norm-conserving scalar relativistic pseudopotentials[10] factorized in the Kleinman-Bylander form.[11] Nonlinear partial-core corrections to describe the exchange and correlations in the core region were included for Mo.[12] We have used a single-ζ basis set including polarization orbitals for Mo atoms, as obtained with an energy shift of 0.02 Ry.[8] We verified that the description of bulk bands for this and related bronzes using this basis size, especially at the Fermi level, is essentially the same as when using a split-valence double-ζ basis set including polarization for all atoms. The energy cutoff of the real space integration mesh was 300 Ry. Calculations for slabs of different thicknesses (containing from one to four octahedral layers) were carried out. For the superlattice we used the structure of Ref. 5 assuming a commensurate value (0.75) of the $\boldsymbol{b}^*$ component of the modulation vector. The Brillouin zone (BZ) was sampled using grids of $(2\times21\times1)$ and $(2\times21\times6)$ k points for the slabs and the bulk, respectively.[13] The energy cutoff and k-points values were tested against well converged values.

The band structure for bulk $Rb_{0.3}MoO_3$ contains two partially filled bands [Fig. 2(a)]. The CDW in this material is due to the interband nesting among these quasi-one-dimensional bands so that the CDW vector, $\boldsymbol{q}_{CDW}$, is given

 ©2006 The American Physical Society

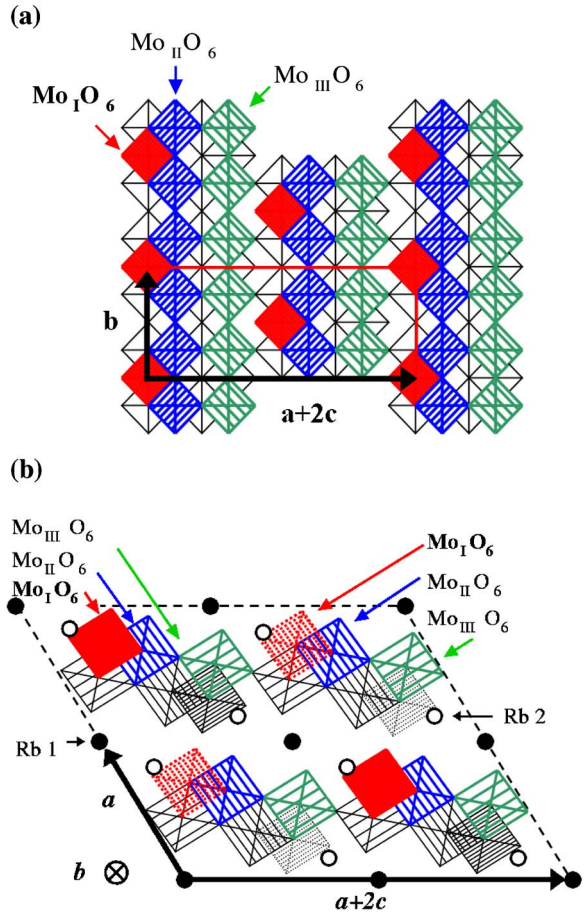

FIG. 1. (Color online) (a) An idealized surface structure of $Rb_{0.3}MoO_3$ in the $(\bar{2}01)$ plane. The filled and dashed square units are in the first MoO_6 sublayer. (b) Idealized sideview of the room temperature $Rb_{0.3}MoO_3$ structure projected onto the plane perpendicular to the $\boldsymbol{b}$ axis. Each square represents a MoO_6 octahedron with the Mo located at the center of oxygen octahedron. Closed circles are Rb atoms at the uppermost positions of the "surface" (labeled 1) and empty circles are Rb atoms 1.2 Å below (labeled 2). The three highest octahedra with respect to the "surface" are the dashed squares indicated by the arrows. Their centers lie at levels 1.8, 2.4, and 3.5 Å below the surface.

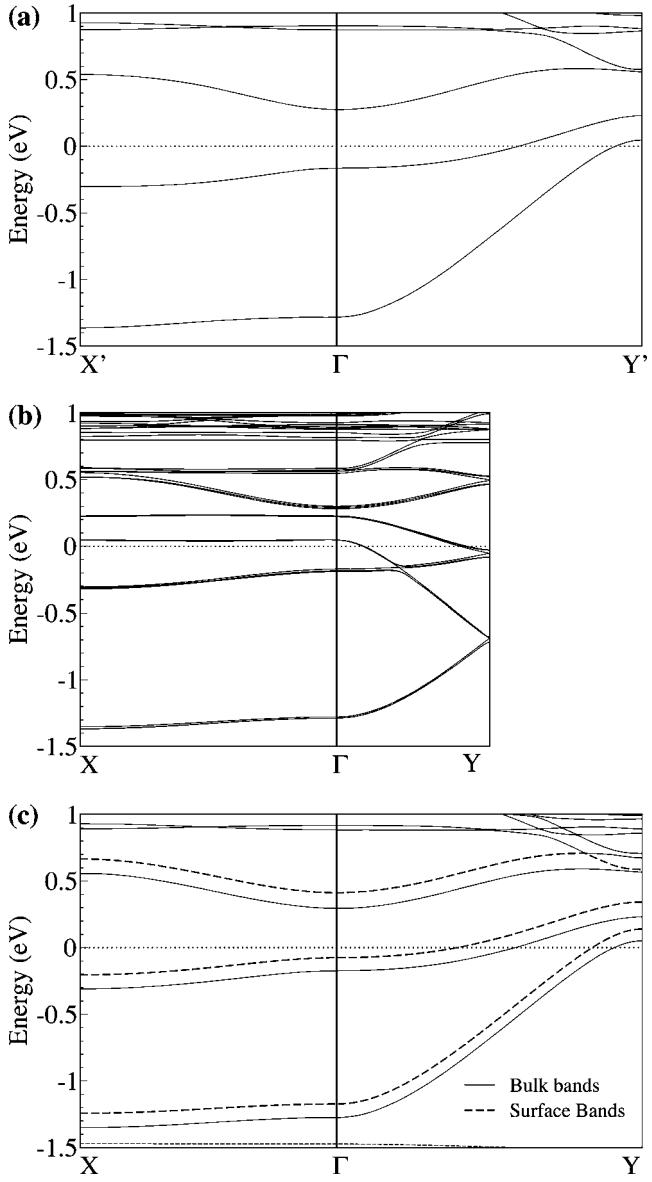

FIG. 2. The band structure for (a) bulk $Rb_{0.3}MoO_3$; (b) a slab preserving the bulk stoichiometry at the surface, and (c) a slab with a defect of Rb atoms (one every three) at the surface. In (a) $\Gamma=(0,0,0)$, $X'=(\frac{1}{2},0,0)$, and $Y'=(0,\frac{1}{2},0)$ in units of the $\boldsymbol{a}'^*$, $\boldsymbol{b}'^*$, and $\boldsymbol{c}'^*$ reciprocal lattice vectors (Ref. 4). In (b) and (c) $\Gamma=(0,0)$, $X=(\frac{1}{2},0)$, and $Y=(0,\frac{1}{2})$ in units of the corresponding oblique reciprocal lattice vectors.

by $\boldsymbol{k}_{f1}+\boldsymbol{k}_{f2}$ where $\boldsymbol{k}_{fi}$ is the Fermi wave vector of band $\boldsymbol{i}$.[14–16] Since there are three electrons per unit cell to fill these bands, a $\boldsymbol{q}_{CDW}$ component along the chain direction of $0.75\boldsymbol{b}^*$ is predicted, which is the observed value at low temperature.[17]

In order to appropriately model the $(\bar{2}01)$ blue bronze surface, we carried out calculations for slabs including different numbers of octahedral (and rubidium) layers, as well as different distributions and concentrations of surface rubidium atoms. There are three rubidium atoms per repeat unit of a layer, two of them [type 2, empty circles in Fig. 1(b)] are very near the octahedral layers and the third one [type 1, full circles in Fig. 1(b)] is equidistant of the two layers. Among these interlayer Rb atoms, only the type-2 Rb atoms closest to the surface and the type-1 Rb atoms might remain at the surface after cleaving the sample. However, due to their position exactly in between the layers, type-1 Rb atoms have on average only 0.5 probablility to remain at the surface after cleavage. Since these atoms are expected to relax from their bulk crystallographic position, we optimized their position with respect to the surface. These positions were the basis for all remaining calculations.

The main conclusions of our calculations were (i) the number of octahedral layers used in the computations is irrelevant; (ii) the key factor in controlling the shape of the surface bands near the Fermi level is the number of Rb atoms at the surface. Shown in Fig. 2(b) is the band structure for a surface which preserves the stoichiometry of the bulk (i.e., 1.5 Rb atoms per repeat unit). Despite the foldedlike shape of the bands, due to the fact that we used a unit cell twice

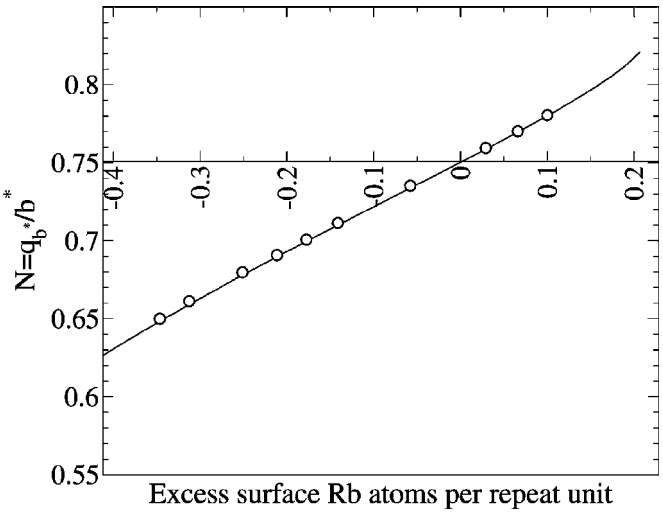

FIG. 3. The $\boldsymbol{b}^*$ component of the surface nesting vector of the $(\bar{2}01)$ surface of rubidium blue bronze versus the density of alkali atoms at the surface. The horizontal axis indicates the number of excess Rb atoms at the surface per unit cell, with the zero corresponding to the stoichiometric Rb composition. The continuous line corresponds to the calculated values. The empty circles refer to the experimental values of $\boldsymbol{q}^*$ probed by STM (See text).

larger along $\boldsymbol{b}$ in order to model the partial occupation of the Rb sites, the partially filled bands are nearly identical to those of the bulk. In contrast, when the repeat unit of the cell at the surface is covered by just one Rb atom, i.e., 0.5 less than in the stoichiometric case, the band structure is noticeably different [Fig. 2(c)]; the corresponding surface bands are shifted upward with respect to those of the bulk. Calculations for the case of an excess of Rb atoms with respect to the stoichiometric situation led to an opposite bandshift. After carrying out computations for several situations, we conclude that different concentrations of Rb atoms at the surface generate a nearly rigid energy shift of the surface bands with respect to those of the bulk. This result has the important implication that the nesting vector at the surface changes with the Rb content. In fact, it is possible to infer the concentration of Rb atoms at the surface that produces a given surface nesting vector, see Fig. 3.

III. EXPERIMENTAL SETUP AND RESULTS

Let us now search for the experimental consequences of this feature. As reported in our previous work[3] we have observed with careful STM experiments the nearly commensurate value of the projection of $\boldsymbol{q}_{CDW}$ onto the $(\bar{2}01)$ plane. Hence, defining $N=\boldsymbol{q}_{b^*}/\boldsymbol{b}^*$ where $\boldsymbol{q}_{b^*}$ is the $\boldsymbol{b}^*$ component of $\boldsymbol{q}_{CDW}$, $N=0.75$ is the bulk reported value and $1\text{-}N=0.25$ is the quantity reported by STM experiments (see parts II and III in Ref. 3). However, it was mentioned that, on some optically flat terraces $1\text{-}N$ was found to deviate from the 0.25 value, yielding inhomogeneities for $\boldsymbol{q}_{b^*}$. We report here experimental results concerning the inhomogeneities of $\boldsymbol{q}_{b^*}$ measured by STM in rubidium blue bronze. Three *in situ* cleaved $Rb_{0.3}MoO_3$ samples from the same batch were investigated with several mechanically sharpened Pt/Ir tips. All samples were prepared in a very similar manner. They were cleaved at room temperature in a UHV and rapidly introduced into the cold STM head. All the STM measurements consisted of constant current mode topographical images and were performed at 77 K or at 63 K, well below the transition temperature ($T_c=180$ K). Optically large and flat plateaus were carefully selected to perform our measurements. Typical experimental conditions were ±450 mV for the applied bias voltage and from 50 to 150 pA for the tunneling current. Much care was taken in order to achieve molecular resolution and CDW resolution with scanning areas ranging from 20×20 nm^2 to 50×50 nm^2. This was necessary to allow accurate measurements of the $1\text{-}N$ ratio for a typical 512×512 pixels image resolution. This $1\text{-}N$ ratio was directly extracted from the two-dimensional (2D) Fourier transform of the STM image. At a given tip location several mesurements were always performed to ensure that the measured $1\text{-}N$ value was reproducible within an error bar of 10%. The main features of the STM images described hereafter as well as the extracted CDW wave vector are found to

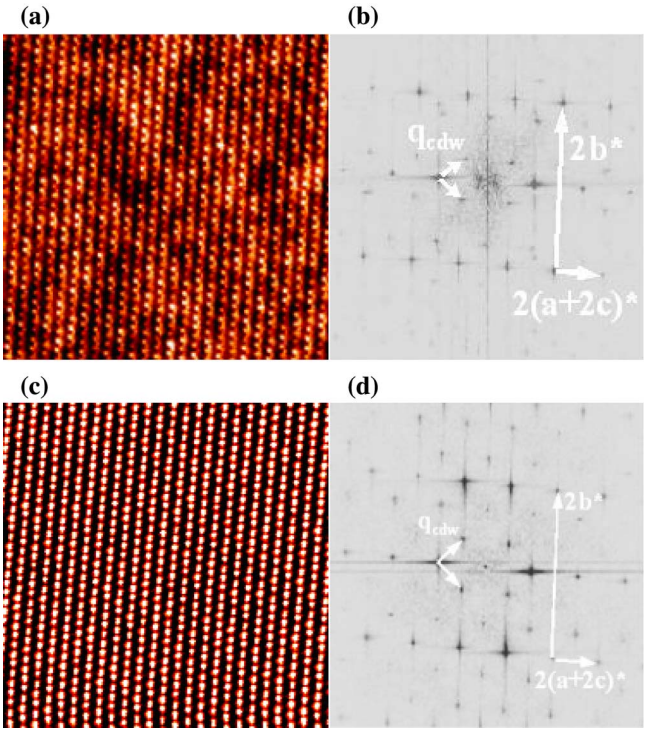

FIG. 4. (Color online) (a) The constant current STM image of about 30×30 nm^2 of an *in situ* cleaved $(\bar{2}01)$ surface of $Rb_{0.3}MoO_3$ in the CDW ground state at 63 K with molecular and CDW resolution. The tunneling conditions are Vbias$=+420$ mV and $I_t=110$ pA. (b) A 2D Fourier transform of (a) showing surface lattice spots indicated by vectors $2\boldsymbol{b}^*$ and $2(\boldsymbol{a}+2\boldsymbol{c})^*$ and CDW superlattice spots around each lattice spot indicated by $\boldsymbol{q}_{CDW}$ short white arrows. In this scanned zone the $\boldsymbol{b}^*$ component of $\boldsymbol{q}_{CDW}$ equals the 0.25 bulk value. (c) The constant current STM image with similar parameters as indicated in (a) but measured on another sample. (d) A 2D Fourier transform of (c) showing the same spots as those appearing in (b) but with the $\boldsymbol{b}^*$ component of $\boldsymbol{q}_{CDW}$ equals 0.30, showing significant clear deviation from the 0.25 bulk value.

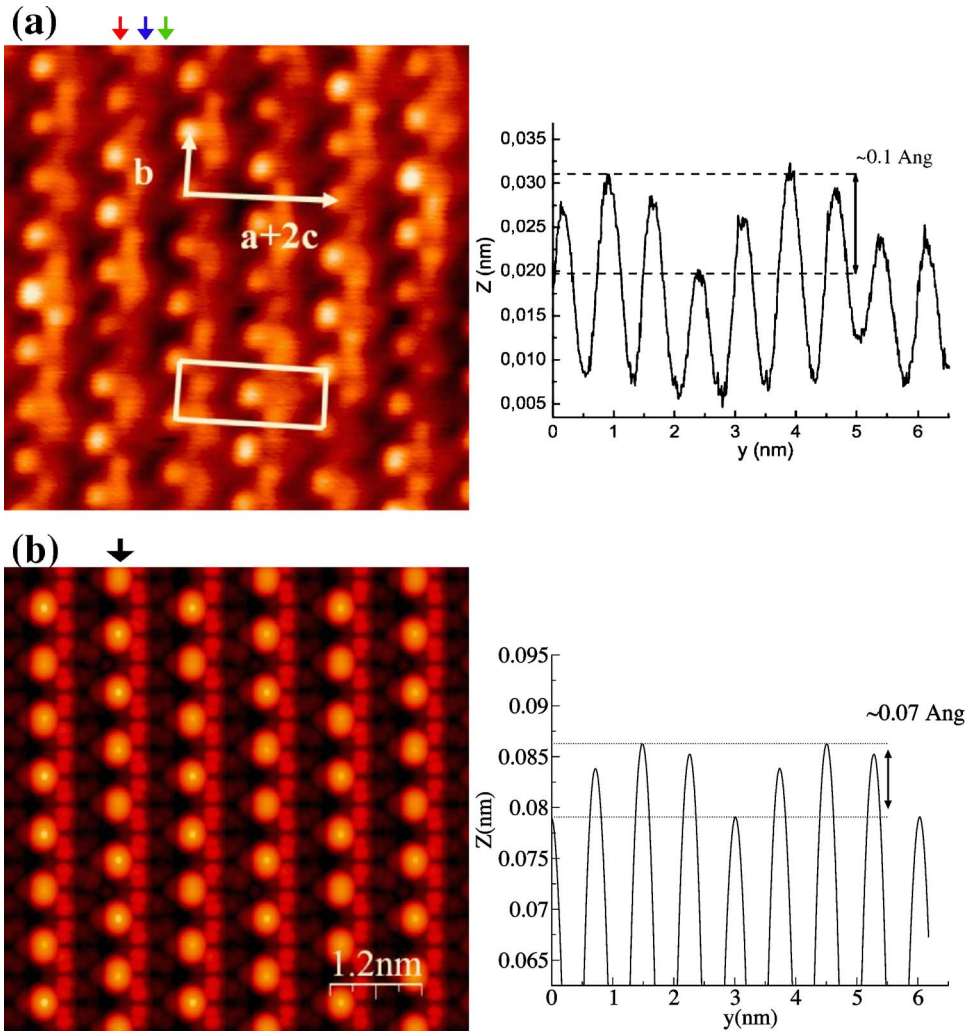

FIG. 5. (Color online) (a) The constant current mode topographical image of 6.2×6.2 nm^2 on $(\bar{2}01)$ plane of $Rb_{0.3}MoO_3$ at 63 K (raw data image). The bias voltage applied on the sample is +420 mV and the set-up tunneling current is 110 pA. Molecular lattice and CDW superlattice coexist in the image. The three arrows indicate (from left to right) , respectively, the observed type I, II MoO_6 octahedra, and the expected position of the $Mo_{III}O_6$ octahedra. An associated profile along Mo_IO_6 octahedra indicated by a left arrow (from Ref. 3). (b) (Color online) The calculated image and associated profile along the Mo_IO_6 octahedra for the modulated phase of $Rb_{0.3}MoO_3$.

be independent upon bias voltage polarity in the above-mentioned energy range.

It is found that optically distinct plateaux (of at least several 100 μm^2 area) could yield distinct values of 1-N significantly different from the 0.25 bulk value. Moreover, on the same plateau, different locations estimated to be at least several μm from each other yielded differences in 1-N values that were much greater than the typical error bar for a single location 1-N measurement, leading to clear deviations of the surface $\boldsymbol{q}_{CDW}$ wave vector with respect to the bulk one projected onto the $(\bar{2}01)$ surface. On the contrary, displacements along $\boldsymbol{b}$ or $\boldsymbol{a}+\boldsymbol{2c}$ on the scale of tens of nanometers from a given position of measurement, did not lead to noticeable changes of $\boldsymbol{q}_{b^*}$. This shows that all measurements were performed far enough from CDW domain boundaries. On the same plateau the greatest change in 1-N value ranged from 0.21 to 0.32. Figure 4 illustrates this situation for STM measurements performed on two different samples with similar imaging conditions; in (a) $N=0.75$, the bulk value and in (c) $N=0.70$. As a result of our study all 1-N values were found in the range 0.21 to 0.35, as indicated by the empty circles in Fig. 3 for the N value.

IV. DISCUSSION

According to the present calculations these inhomogeneities would correspond to an excess of surface alkali atoms ranging from about 0.1 to −0.35 per repeat unit. These predictions would then be consistent with the hypothesis that the distribution of type-1 alkali atoms is mainly responsible for the experimental deviations observed in the CDW wave vector value at the surface. The effect on the electronic properties induced by losing surface alkali atoms has been studied by photoemission combined with Ne ions sputtering.[18] It was found that alkali desorption decreases the electronic spectral weight around the Fermi level (Ef) and shifts away from Ef the onset of the valence band. Our experimental and theoretical studies are consistent with these observations.

On the other hand the present results could seem in disagreement with angular resolved photoemission spectroscopy (ARPES) and grazing x-ray diffraction, showing both that N almost equals 0.75 under 100 K. [19,20] This is because STM probes $\boldsymbol{q}_{CDW}$ only at the uppermost layer of the compound and very locally at the nanometer scale inside a single CDW domain. Both x-ray and ARPES experiments probe $\boldsymbol{q}_{CDW}$ over a macroscopical in-plane scale and over deeper

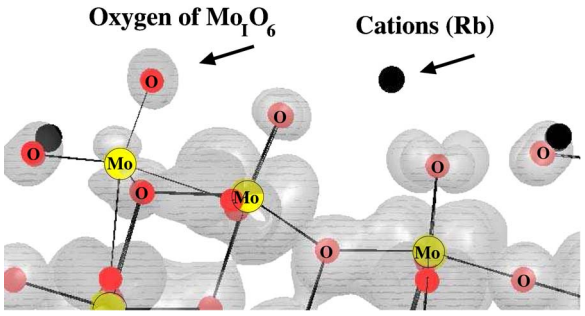

FIG. 6. (Color online) The isocharge density, represented as the gray surface [sideview as in Fig. 1(b)] integrated from the Fermi level to 0.5 eV above. All the relevant atoms have been labeled. In the image in color the Rb, Mo, and O atoms are shown as black, yellow (light gray), and red (gray) balls, respectively.

layers (for x-ray), which remain unaffected by the inhomogeneities present in the first layer, according to the present calculations. This leads to an averaged value of $\boldsymbol{q}_{CDW}$ in a macroscopical volume showing no surface inhomogeneities.

We now turn to the analysis of the main features of the STM images for the modulated phase of $Rb_{0.3}MoO_3$ in stoichiometric conditions. As shown in Fig. 5 where the chains along $\boldsymbol{b}$ are readily visible, there is a very good agreement between the experimental and calculated[22] images. The observed STM pattern inside the surface elementary unit cell contains two features (one well-defined ball next to a more elongated continuous pattern along $\boldsymbol{b}$) which were attributed[3] to the Mo_IO_6 and $Mo_{II}O_6$ octahedra, respectively.

In order to better understand these images we report in Fig. 6 a plot of the isocharge density integrated from the Fermi level to 0.5 eV above. Two features must be noted. First, there is essentially no contribution of the Rb atoms. This provides computational support for the suggestion that the STM measurement is not sensitive to them.[21] Second, the density is noticeable around the outer O atom of the Mo_IO_6 octahedra. These O atoms are the uppermost part of the surface, those of the $Mo_{II}O_6$ octahedra staying approximately 0.6 Å below. These two facts together easily explain why the brightest spots originate from the outer O atom of the Mo_IO_6 octahedra. In addition, the amplitude of the bulk vertical displacement of the outer O atom of the Mo_IO_6 octahedra in the modulated structure used in the calculation is between three and four times smaller than the amplitude of the calculated density profile along the Mo_IO_6 octahedra [Fig. 5(b)]. This means that the STM experiment is mostly measuring the differences in the local density of states (LDOS) associated with these O atoms, as a result of the existence of the CDW and not the differences in height of these atoms. The above-mentioned apparent contradiction with previous works is solved by the results of Fig. 6. Around 42.5% of the charge density in this figure is associated to Mo_{II}, 22.1% to Mo_{III}, 1.9% to Mo_I, and 1.2% to the outer O of the Mo_IO_6. Consequently, the CDW modulation mostly affects the Mo_{II} and Mo_{III} atoms. However, because of the nonnegligible participation of the outer O atoms of the Mo_IO_6 octahedra, as a result of the strong hybridization between the Mo and O orbitals, the orbital mixing associated with the CDW modulation affects the LDOS of these atoms, leading to the differences in the profile of Fig. 5. According to the present results the more continuous path must originate not only from the outer O atoms of the $Mo_{II}O_6$ octahedra, but also from the Mo_{II} atoms which strongly participate in the wave function. However the difference in height with respect to the uppermost part of the surface leads to the considerably less intense signal. Finally, the $Mo_{III}O_6$ octahedra, which lie considerably deeper (i.e., approximatly 1.7 Å lower than the Mo_IO_6 octahedra) are not visible at all in the STM image, even though the CDW modulation strongly affects them.

V. CONCLUSION

In summary, a combined theoretical-experimental approach has led to an in-depth understanding of the STM observation for the CDW in quasi-one-dimensional blue bronze. The discrepancy between how the CDW is revealed in STM and x-ray experiments has been understood. The decisive role played by the surface Rb atoms, leading to experimental surface CDW vector inhomogeneities, has been clarified.

ACKNOWLEDGMENTS

Work at Bellaterra was supported by DGI-Spain (Project BFM2003-03372-C03), Generalitat de Catalunya (2005 SGR 683), CSIC (I3P-BPD2001-1) and by grants for computer time from the CESCA-CEPBA. Work at Marcoussis was supported by Région Ile de France (SESAME project n° 1377) and by Conseil Général of Essone. We would like to thank J-C. Girard, C. Schlenker, J. Dumas, D. Le Bolloc'h, S. Ravy, S. Brazovskii, and N. Kirova for helpful discussions. The technical assistance of C. David is greatly acknowledged. E.M.-C. acknowledges financial support from the Institut Català de Nanotecnologia.

*Author to whom correspondence should be addressed; email: canadell@icmab.es

[1] For reviews see *Low Dimensional Electronic Properties of Molybdenum Bronzes and Oxides*, edited by C. Schlenker (Kluwer, Dordrecht, 1989); *Physics and Chemistry of Low Dimensional Inorganic Conductors*, edited by C. Schlenker, J. Dumas, M. Greenblatt, and S. van Smaalen, NATO Advanced Studies Institute, Series B: Physics (Plenum, New York, 1996), Vol. 354; J. Dumas and C. Schlenker, Int. J. Mod. Phys. B **7**, 4045 (1993).

[2] J. Graham and A. D. Wadsley, Acta Crystallogr. **20**, 93 (1966).

[3] C. Brun, J. C. Girard, Z. Z. Wang, J. Marcus, J. Dumas, and C. Schlenker, Phys. Rev. B **72**, 235119 (2005).

[4] J. L. Mozos, P. Ordejón, and E. Canadell, Phys. Rev. B **65**, 233105 (2002).

[5] W. J. Schutte and J. L. D. Boer, Acta Crystallogr., Sect. B: Struct. Sci. **49**, 579 (1993).

[6] P. Hohenberg and W. Kohn, Phys. Rev. **136**, B864 (1967).
[7] W. Kohn and L. J. Sham, Phys. Rev. **140**, A1133 (1965).
[8] J. M. Soler, E. Artacho, J. D. Gale, A. García, J. Junquera, P. Ordejón, and D. Sanchez-Portal, J. Phys.: Condens. Matter **14**, 2745 (2002).
[9] J. P. Perdew, K. Burke, and M. Ernzerhof, Phys. Rev. Lett. **77**, 3865 (1996).
[10] N. Troullier and J. L. Martins, Phys. Rev. B **43**, 1993 (1991).
[11] L. Kleinman and D. M. Bylander, Phys. Rev. Lett. **48**, 1425 (1982).
[12] S. G. Louie, S. Froyen, and M. L. Cohen, Phys. Rev. B **26**, 1738 (1982).
[13] H. J. Monkhorst and J. D. Pack, Phys. Rev. B **13**, 5188 (1976).
[14] J. P. Pouget, C. Noguera, A. H. Moudden, and J. Moret, J. Phys. (Paris) **46**, 1731 (1985).
[15] M.-H. Whangbo and L. F. Schneemeyer, Inorg. Chem. **25**, 2424 (1986).
[16] G.-H. Gweon, J. W. Allen, R. Claessen, J. A. Clack, D. M. Poirier, P. J. Benning, C. G. Olson, W. P. Ellis, Y.-X. Zhang, L. F. Schneemeyer *et al.*, J. Phys.: Condens. Matter **8**, 9923 (1996).
[17] J. P. Pouget, S. Kagoshima, S. Schlenker, and C. Marcus, J. Phys. (Paris), Lett. **44**, L113 (1983).
[18] K. Breuer, K. E. Smith, M. Greenblatt, and W. McCarroll, J. Vac. Sci. Technol. A **12**, 2196 (1994).
[19] A. V. Fedorov, S. A. Brazovskii, V. N. Muthukumar, P. D. Johnson, J. Xue, L.-C. Duda, K. E. Smith, W. H. McCarroll, M. Greenblatt, and S. L. Hulbert, J. Phys.: Condens. Matter **12**, L191 (2000).
[20] X.-M. Zhu, R. Moret, H. Zabel, I. K. Robinson, E. Vlieg, and R. M. Fleming, Phys. Rev. B **42**, 8791 (1990).
[21] U. Walter, R. E. Thomson, B. Burk, M. F. Crommie, A. Zettl, and J. Clarke, Phys. Rev. B **45**, 11474 (1992).
[22] The images were calculated using the Tersoff-Hamann approximation [J. Tersoff and D. R. Hamann, Phys. Rev. Lett. **50**, 1998 (1983); Phys. Rev. B **31**, 805 (1985)] in which the tunneling current is proportional to the local density of states integrated from the Fermi level to the bias voltage.